Vehicle pass-by noise auralization in a virtual urban environment

Christian Dreier[1], Michael Vorländer[2]
Institute for Hearing Technology and Acoustics, RWTH Aachen University
Kopernikusstraße 5, 52074 Aachen, Germany

ABSTRACT

Auralization is a suitable method for the subjective evaluation of environmental noise. Due to its complexity, the plausible and immersive acoustic representation of outdoor scenarios in urban environments is an ongoing field of research. This work presents the design and implementation of a vehicle pass-by noise model with application in a spatial environmental noise auralization and visualization framework. The acoustic sources are implemented by procedural audio syntheses of engine and road-tyre noise with according directivities. For audio-visual demonstrations, the resulting source model is auralized considering the sound propagation phenomena in a virtual urban environment using the Virtual Acoustics framework.

1. INTRODUCTION

1.1. Background

Auralization of complex urban scenarios is a promising, but technically challenging approach. From a theoretical point of view, urban noise auralization deals with inherent non-LTI (i.e. linear time-variant) properties of the propagation medium (air) that occurs due to turbulence-induced advection as well as refraction due to temperature, humidity and pressure inhomogeneities. As exemplarily shown in a recent publication [1] and demonstrated in an according 360° video[3], environmental noise studies can be performed in Virtual Reality (VR). An auralization usually consists of separated simulation models for sources, propagation and receivers [2]. Especially for psychoacoustic perception studies of noise sources – such as aircrafts, cars or trains – the acoustic source models should reproduce spectro-temporal characteristics and enable dynamic parameter control for enhanced plausibility. Traffic noise auralization approaches based on simulated sources have been performed e.g. in the LISTEN project [3]. The model combines a pre-calculated road-tyre noise component and additive harmonics for the engine component. Furthermore, the model is enhanced by horizontal directivities in the frequency range up to 8 kHz. Based on this signals, the propagation simulation for fixed, pre-calculated positions – in combination with measurement-based [4] or simulated propagation path impulse responses using the pseudo-spectral time domain method (PSTD) [5] – have been

[1]cdr@akustik.rwth-aachen.de

[2]mvo@akustik.rwth-aachen.de

[3]https://www.youtube.com/watch?v=rudxfV94UwA&list=PLjVMT5BkCe83h299e3FWNivk-MFtRnpw-&index=2

performed. Recently, a framework that includes visualization was developed by researchers at the University of York [6]. In this approach, different tools – Unity3D, Pure Data, Wwise, and Matlab – are concatenated with the underlying vehicle pass-by model being based on the analytic horizontal directivity description from the HARMONOISE catalogue [7] and the propagation effect simulation assuming a first order image source of a sound hard ground.

1.2. Contribution

With regard to compatibility to the open-source Virtual Acoustics auralization software (VA) [8] and according real-time constraints, this work presents a vehicle pass-by noise model for dynamic, real-time auralizations. To the research field on environmental noise auralizations, the presented approach further contributes a spatial directivity encoding using the OpenDAFF file format [9]. The sound propagation including directivity-dependent reflections and diffractions of building surfaces are calculated based on the image edge model [10]. The framework enables rendering to multiple spatial headphone- or loudspeaker-based reproduction systems. Due to the server-based nature of *Virtual Acoustics* the framework can be connected to visualization engines, such as Unity3D or Unreal Engine.

2. AURALIZATION MODEL

The VA framework is following a three-step paradigm of discrete source-propagation-receiver models. The following block diagram (fig.1) includes a parameter overview of environmental noise auralization in VA.

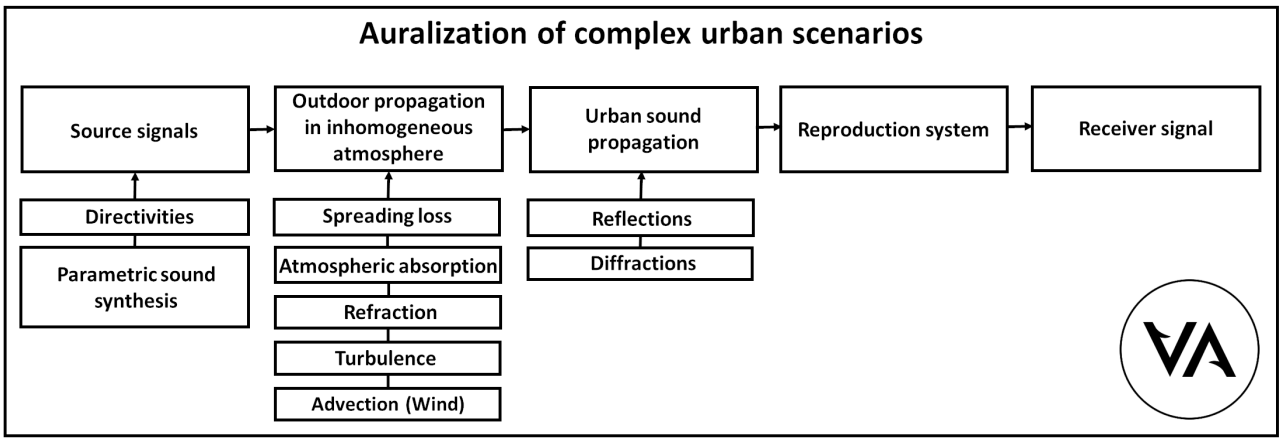

Figure 1: Block diagram of environmental noise auralization in VA.

2.1. Source model of vehicle pass-by noise

The source model is subdivided into an omnidirectional and a higher-order directional component. The latter component is coded into a file using the OpenDAFF format [9]. The source model is obtained from an inverse modelling method, described in [11]. The inverse method focuses on the measurement and calculation of acoustic far-field directivities of moving sources. In such a far-field directivity some effects on the wave propagation are included that cannot easily be simulated even with elaborated numerical methods and therefore have to be measured:

- Advection due to the object speed and the laminar flow around the moving object;
- Refraction due to turbulent flow at body cavities;
- Diffraction due to object geometry;

– Scattering due to surface roughness (of asphalt) that in turn influences both sound generation mechanism and the near-field propagation.

In order to obtain a directivity that is comparable to free-field conditions, the measured signals from the pass-by are corrected for

– an image source that appears due to the surface impedance,

– the geometrical distance law-dependent loss, and

– the air absorption between the measurement point and the virtual directivity hull of the moving object.

The resulting omnidirectional road-tyre noise component spectrum and the higher-order directivity is shown in fig.2.

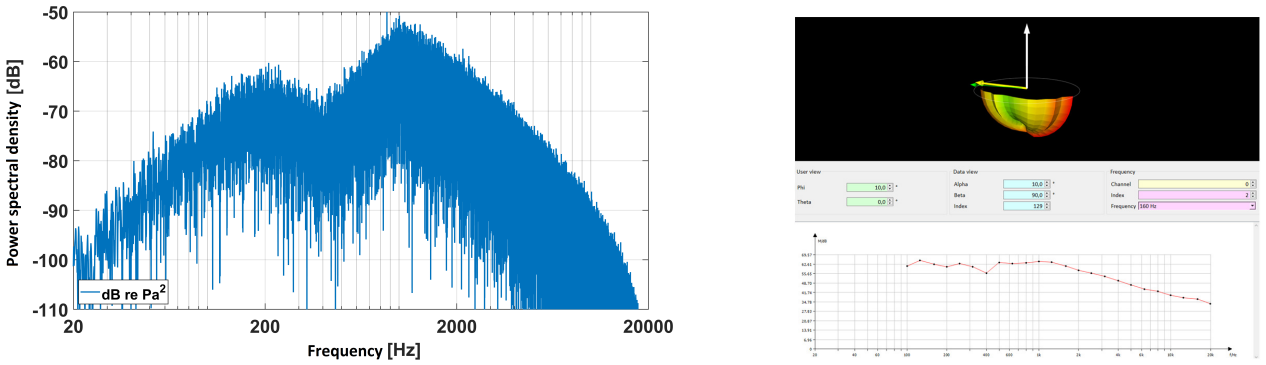

Figure 2: Synthesized road-tyre noise component (left) and higher-order directivity component, shown in the *OpenDAFF Viewer* (right).

For parameterization and virtual reality implementations, the obtained directivities must be based on speed-dependent data. If measurement-based directivities are not available, engineering models of different level of detail can be applied, such as an easier model from the HARMONOISE catalogue [7] or the more complex SPERoN model [12].

2.2. Sound propagation model

Source extension-dependent spreading loss

The block diagram (fig.1) enumerates the outdoor sound propagation effects to be considered by ISO 9613-2 [13]. With regard to the spreading loss factor, a finite line source – such as a car with a line length equal to its wheelbase – behaves as that from an infinite line (cylindrical spreading) due to wavefront spreading at distances much less than the length of the source and as that from a point source (spherical spreading) at distances greater than the length of the source (fig.3).

Boundary conditions at the ground

The sound field at the receiver can be assumed as a superposition of the direct and the reflected wave. In the case of vehicle noise emissions, the ground reflection has the greatest influence on the acoustic far field. Depending on the ground material, the delay and amplitude of the reflected wave is affected due to the frequency-dependent absorption coefficients. In order to compare the influence of a (noise-reducing) porous with a non-porous asphalt surface the sound field is simulated in the following using different ground material properties.
In the case of a non-locally reacting ground such as porous asphalt, the frequency-dependent absorption coefficient of a material α is derived from its plane-wave reflection coefficient R_p based

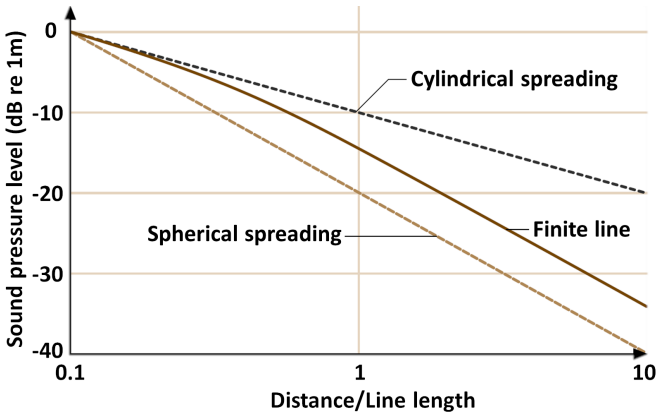

Figure 3: Distance-dependent spreading loss of spherical, cylindrical an finite line sound sources. Modified from [14].

on the geometry-dependent complex surface impedance Z_s, the complex characteristic ground impedance Z_c, complex wave number k, $k_0 = 2\pi f/c$ (c being the homogeneous sound speed of air), its layer thickness d and the grazing angle Θ by

$$\alpha = 1 - |R_p|^2 \tag{1}$$

with

$$R_p = \frac{Z_s \sin\Theta - \chi}{Z_s \sin\Theta + \chi} \tag{2}$$

with

$$\chi = [1 - (k_0/k)^2 \cos^2\Theta]^{1/2} \tag{3}$$

and (assuming a rigid-backed layer)

$$Z_s = Z_c \cdot \coth(-ikd). \tag{4}$$

Z_c and k are resulting from the above-mentioned Hamet [15] and Miki [16] model equations for equivalent fluids. Whereas the phenomenological Hamet model depends on three parameters (flow resistivity R_s, porosity Ω and tortuosity q^2, the Miki model merely depends on R_s. Compared to the more popular *Delany-Bazley* model equations, the Miki expressions perform better in particular for the very low frequency range $f/R_s < 0.01$ for double layer impedances. The Hamet model equations are:

$$Z_c = \rho_0 c_0 \frac{1}{\Omega} \sqrt{\frac{K}{\gamma}} \frac{\sqrt{1 - i\frac{f_\mu}{f}}}{\sqrt{1 - (1 - \frac{1}{\gamma})\frac{1}{1 - i\frac{f_\Theta}{f}}}} \tag{5}$$

and

$$k = k_0 \sqrt{K\gamma} \sqrt{1 - i\frac{f_\mu}{f}} \sqrt{1 - (1 - \frac{1}{\gamma})\frac{1}{1 - i\frac{f_\Theta}{f}}} \tag{6}$$

where $\rho_0 c_0$ is the specific wave impedance in air, $\gamma = c_p/c_v = 1.4$ is the classical ratio of specific heats for air, $f_\mu = \frac{1}{2\pi}\frac{R_s}{\rho_0}\frac{\Omega}{K}$ and $f_\Theta = \frac{1}{2\pi}\frac{R_s}{\rho_0}\frac{1}{N_{pr}}$ – with $N_{pr} = 0.71$ being the Prandtl number for air – are characteristic frequencies associated to the viscous and thermal effects respectively. The theoretical prediction are plotted in fig.4. The asphalt surface impedance is calculated assuming a rigid-backed layer with a thickness $d = 0.04$m.

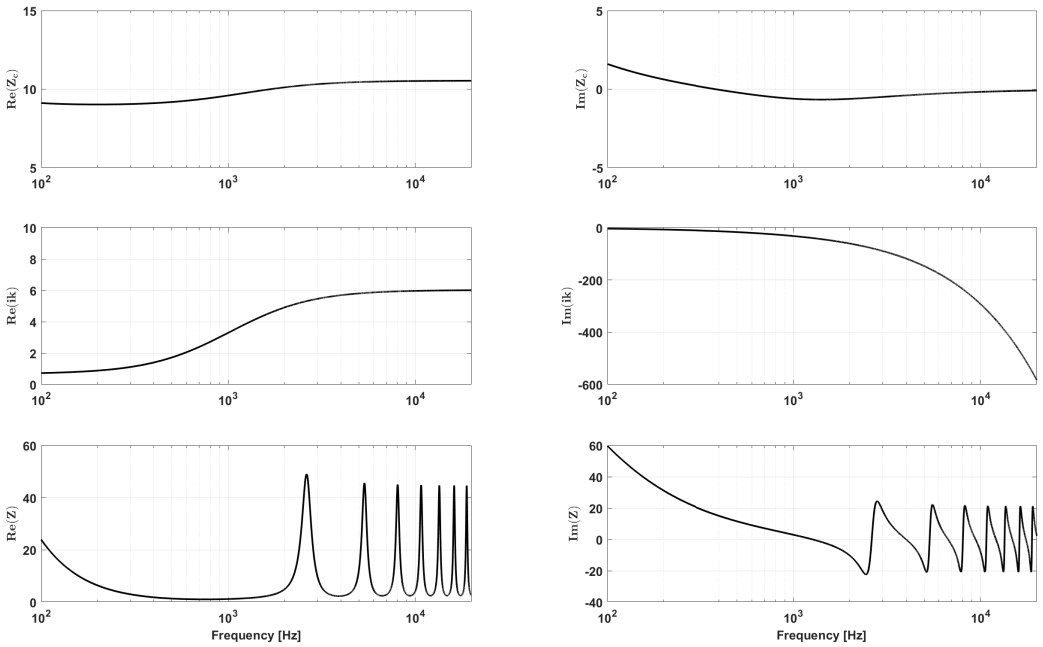

Figure 4: Theoretical predictions for porous asphalt based on the *Hamet* model equations for parameters $R_s = 5000\frac{\mathrm{Ns}}{\mathrm{m}^4}$, $\Omega = 15\%$, and $q^2 = 2.5$: (a) characteristic impedance Z_c, (b) propagation constant ik, and (c) surface impedance Z_s.

In the case of non-porous asphalt a flow resistivity value R_s for stone mastic asphalt (SMA) was taken from literature ($R_s = 6 \cdot 10^7 \frac{\mathrm{Ns}}{\mathrm{m}^4}$). The ground impedance yields

$$Z_c = \rho_0 c_0 \left[1 + 5.5\left(10^3 \frac{f}{R_s}\right)^{-0.632} - j8.43\left(10^3 \frac{f}{R_s}\right)^{-0.632}\right] \tag{7}$$

and the complex wave number yields

$$k = k_0 \left[1 + 7.81\left(10^3 \frac{f}{R_s}\right)^{-0.618} - j11.41\left(10^3 \frac{f}{R_s}\right)^{-0.618}\right]. \tag{8}$$

The resulting frequency-dependent absorption coefficient (fig.5) shows good agreement with impedance tube measurement results from literature (fig.5 in [17]). The high absorption coefficient of porous asphalt at 1 kHz might explain the noise-reducing effectiveness of such surfaces since the *Horn effect* of the road-tyre noise component as major contribution in this frequency range might be suppressed.

Based on both absorption coefficients, the impact on the sound propagation transfer functions can be calculated (fig.6). From a theoretical point of view, this problem is that of sound propagation along an impedance plane and is implemented as comprehensively discussed in [18]. This approximation – that was obtained by numerical double saddle point method of integration from an analytic form assuming a spherical wave as infinite number of plane waves – is valid for $k_0 r_2 \gg 1$ where r_2 is the source-receiver distance of the ground-reflected wave, small grazing angles $\cos\Theta \ll 1$ and hard boundaries $|\beta|^2 \ll 1$ where $\beta = Z_0/Z_s$ is the specific acoustic admittance ratio of the surface. Mathematically, the plane-wave reflection coefficient R_p in equation (2) is modified to

$$Q = R_p + (1 - R_p)F(w) \tag{9}$$

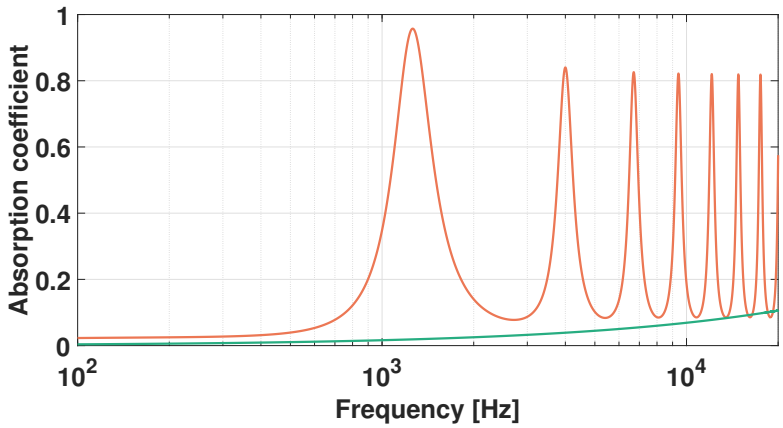

Figure 5: Absorption coefficients for rigid-backed 4-cm-thick porous asphalt, obtained from the *Hamet* model (orange) for values of $R_s = 5000\frac{\text{Ns}}{\text{m}^4}$, $\Omega = 15\%$, and $q^2 = 2.5$, and for non-porous asphalt obtained from the *Miki* model (green) for a flow resistivity of $R_s = 6 \cdot 10^7 \frac{\text{Ns}}{\text{m}^4}$.

where Q is the spherical reflection coefficient of the ground. The term $(1 - R_p)F(w)$ accounts for a *surface wave* component, where

$$F(w) = 1 + i\sqrt{\pi}w \exp(-w^2)\,\text{erfc}(-iw). \tag{10}$$

In this equation a virtually extended reaction surface is described by

$$w^2 = 2ik_0 r_2 \chi^2 \left[Z_{\text{norm}}(1 - R_p)\right]^{-2} \tag{11}$$

using the normalized surface impedance $Z_{\text{norm}} = Z_s/Z_0$. The high absorption coefficient of porous asphalt at multiple harmonic frequencies leads to a theoretical noise reduction of $5 - 6$dB at the receiver, compared to a conventional stone mastic asphalt layer (fig.6).

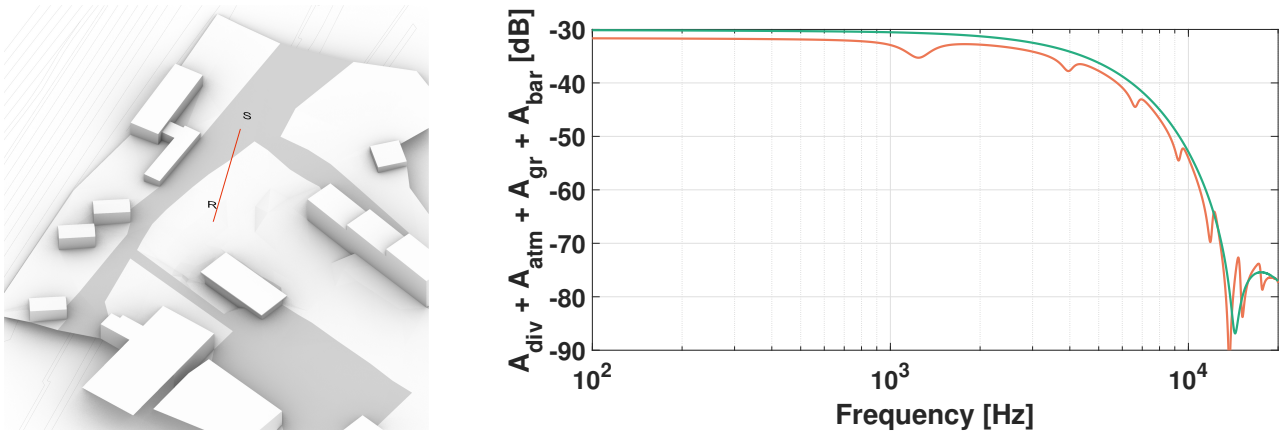

Figure 6: Influence of different ground materials on excess attenuation between a source S and a receiver R based on the material properties of porous (orange) and non-porous asphalt (green) as shown in fig.5.

Higher order reflections and diffractions

As in room acoustics simulation, the sound propagation in urban environments can be based on measured or simulated methods. The biggest challenge for real-time outdoor sound propagation simulations are the big number of reflected and diffracted paths that propagate over very large distances – up to several kilometers at the example of aircraft noise. Aiming at real-time auralization,

the calculation of the numerical solution of the wave equation (so-called *wave-based acoustics*) is too computationally expensive for the audible frequency range, so that in this study, the auralization is based on the assumptions of *geometrical acoustics*. One algorithm of geometrical acoustics is ray tracing. Here, rays are launched from the sound source in every direction and traced until they hit a sphere around a receiver, or their energy has decayed below a given threshold. Along a found ray path, acoustic properties can be calculated based on the associated rays. Since diffraction cannot directly be simulated by GA methods, modified diffraction models based on asymptotic formulations – where infinite edge's contribution (the diffraction wave emanating from the edge) are described by an explicit expression – can be used for efficient computation, e.g., the Uniform Theory of Diffraction (UTD) [19]. An open-source tool for finding sound paths in an urban environment including higher-order reflections and diffractions from a building's surfaces and edges by computation of a deterministic solution to this problem based on the image edge model was developed by Erraji [10]. The reflection and diffraction paths in the IHTApark scene are shown in fig.7 for different simulation orders.

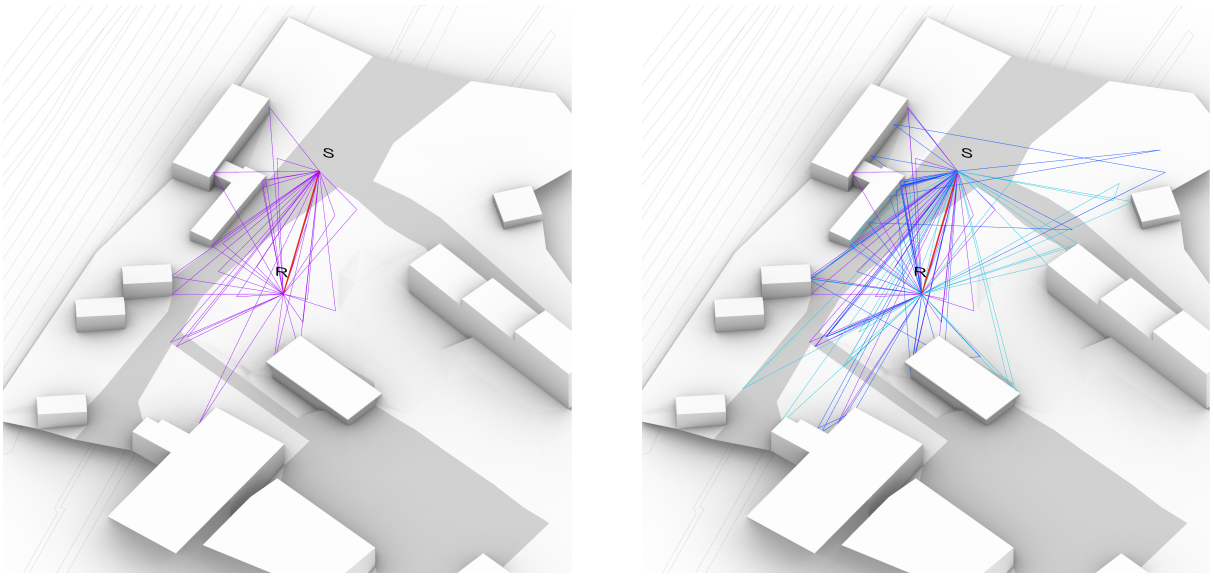

Figure 7: Simulated acoustic propagation paths between a source S and a receiver R for different reflection and diffraction orders (r | d) in the IHTApark model (see [1]). Left: (1|1), right: (2|2).

The higher order reflection and diffraction paths in an urban environment are added at the receiver and contribute with individual delays and amplitudes to the overall impulse response shown in fig.8 (left). The according transfer function (right) can be compared to the previously discussed excess attenuation in fig.6.

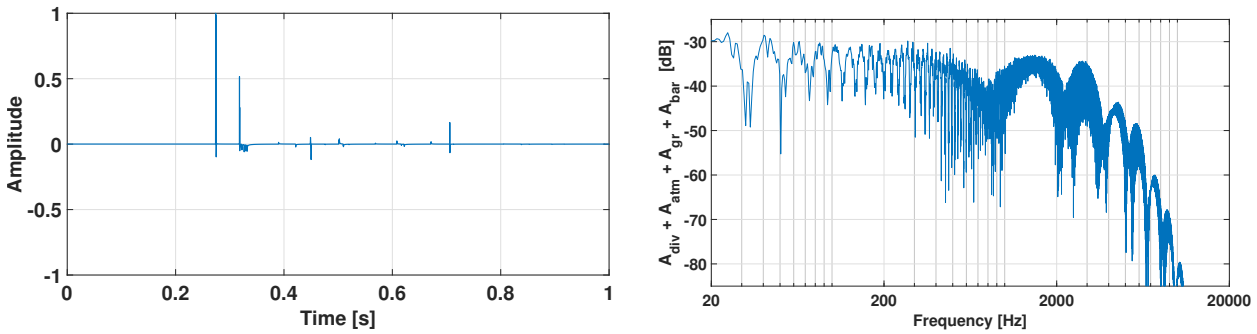

Figure 8: Impulse response (left, normalized) and according transfer function (right) between the positions of source S and receiver R from the scenario in fig.7.

3. CONCLUSIONS

A framework for auralization of urban soundscapes was described. First results were presented in video demonstrations. The framework is subject to ongoing work with an extension towards a larger variety of types of sources. For vehicle pass-by, results are promising which can be expected from the implementation of virtual street vehicles in urban scenes. The interaction with road surfaces is under investigation, whereas the sound propagation components of reflections and diffractions in the built environment are well established but parameter settings can still be optimized.
Concerning outlook to further work, subjective assessments of noise countermeasures in the urban environment – such as porous asphalt vs. conventional non-porous asphalt – can hence be implemented and evaluated using auralizations. In the scope of environmental noise auralization several research directions exist: With respect to real-time constraints it is necessary to omit the simulation of high-order propagation paths. These culling strategies can be based on perception-based thresholds where according rules must be further studied. With regard to computational optimization should be perceptually evaluated if the consideration of spherical wave reflection coefficients, i.e. eqs. (9) – (11) is audible or can be neglected.

ACKNOWLEDGEMENTS

The authors like to thank the HEAD-Genuit Foundation (ID P-22/02-W) for funding this research.

REFERENCES

[1] M. Llorca-Bofí, C. Dreier, J. Heck, and M. Vorländer. Urban sound auralization and visualization framework – Case study at IHTApark. *Sustainability*, 14:2026, 2022.

[2] M. Vorländer. *Auralization. Fundamentals of Acoustics, Modelling, Simulation, Algorithms and Acoustic Virtual Reality. 2nd ed.* Springer, 2020.

[3] J. Forssén, T. Kaczmarek, J. Alvarsson, P. Lundén, and M. Nilsson. Auralization of traffic noise within the listen project – preliminary results for passenger car pass-by. In *EURONOISE – 8th European Conference on Noise Control*, volume 31, 2009.

[4] F. Georgiou, M. Hornikx, and A. Kohlrausch. Auralization of a car pass-by inside an urban canyon using measured impulse responses. *Applied Acoustics*, 183, 2021.

[5] F. Georgiou, M. Hornikx, and A. Kohlrausch. Auralization of a car pass-by using impulse responses computed with a wave-based method. *Acta Acustica united with Acustica*, 105(2):381–391, 2019.

[6] Y. Fu. *Auralisation of Trac Flow using Procedural Audio Methods*. PhD thesis, University of York, 2021.

[7] H. Jonasson. Acoustical source modelling of road vehicles. *Acta Acustica united with Acustica*, 93(2):173–184, 2007.

[8] Institute for Hearing Technology and Acoustics, RWTH Aachen University. Virtual Acoustics – a real-time auralization framework for scientific research. http://www.virtualacoustics.org.

[9] Institute for Hearing Technology and Acoustics, RWTH Aachen University. OpenDaff – Open directional audio file format. http://www.opendaff.org.

[10] A. Erraji, J. Stienen, and M. Vorländer. The image edge model. *Acta Acust.*, 5:17, 2021.

[11] C. Dreier, J. Hahn, and M. Vorländer. Inverse modelling of vehicle pass-by noise for auralizations. *Proc. DAGA – Fortschritte der Akustik*, 48:1455–1458, 2022.

[12] T. Beckenbauer, P. Klein, J. Hamet, and W. Kropp. Tyre/road noise prediction: A comparison between the SPERoN and HyRoNE models - part 1. *Journal of the Acoustical Society of America*, 123:3388–3388, 2008.

[13] Acoustics – attenuation of sound during propagation outdoors – part 2: General method of calculation. ISO 9613-2:1996, International Organization for Standardization, Geneva, CH, 1996.

[14] K. Attenborough. *Sound Propagation in the Atmosphere*, pages 117–155. Springer New York, New York, NY, 2014.

[15] M. Bérengier, M. Stinson, G. Daigle, and J. Hamet. Porous road pavements: Acoustical characterization and propagation effects. *J. Acoust. Soc. Am.*, 101(1):155–162, 1997.

[16] Y. Miki. Acoustical properties of porous materials-modifications of Delany-Bazley models. *Journal of the Acoustical Society of Japan (E)*, 11(1):19–24, 1990.

[17] V. Vázquez, F. Terán, J. Luong, and S. Paje. Functional performance of stone mastic asphalt pavements in spain: Acoustic assessment. *Coatings*, 9(2), 2019.

[18] C. Chien and W. Soroka. Sound propagation along an impedance plane. *Journal of Sound and Vibration*, 43(1):9–20, 1975.

[19] R. Kouyoumjian and P. Pathak. A uniform geometrical theory of diffraction for an edge in a perfectly conducting surface. *Proc. IEEE*, 62(11):1448–1461, 1974.